A Concept of Radial Pseudo-Force for Damage Detection in Wind Turbine Towers

WEI XU, MAOSEN CAO, ZHONGQING SU
and WIESLAW OSTACHOWICZ

ABSTRACT

Damage in a plane structure can cause perturbation to the equation of out-of-plane motion, which can be equivalently regarded as the transverse pseudo-force (TPF) applied to the plane structure. Thereby, the detection of damage in the plane structure can be achieved by identifying the TPF. Nevertheless, it is difficult to formulate the pseudo-force in a cylinder structure such as a wind turbine tower because its radial, longitudinal, and circumferential motions are coupled. The aforementioned limitation leads to a noticeable barrier to extending the TPF to a cylinder structure. To overcome this barrier, a new concept of radial pseudo-force (RPF) is formulated to represent the damage-caused perturbation to the radial equilibrium of a cylinder structure, whose motions are dominated by radial components. The RPF is applied on the lateral surface of the cylinder and is an ideal indicator for the detection of damage in the cylinder structure because it appears in the damage region only and almost vanishes in intact locations. The concept of the RPF is experimentally validated on a wind turbine tower model, on the internal surface of which a pit was manufactured. The results reveal that the RPF-based approach is capable of detecting internal damage in cylinder structures such as wind turbine towers by graphically characterizing the occurrence, location, and size of the damage.

INTRODUCTION

Many structural components one can encounter in real applications like wind turbine towers can be simplified as cylinders [1]. With the motivation of ensuring the integrity and safety of cylinders, nondestructive testing (NDT) techniques relying on electrical resistance, thermography, electro-mechanical impedance, laser ultrasonic, strain, etc., have been applied for the detection of damage [2-6].

Wei Xu, Hohai University, 1 Xikang Road, Nanjing 210098, China. Maosen Cao, Hohai University, 1 Xikang Road, Nanjing 210098, China
Zhongqing Su, The Hong Kong Polytechnic University, Kowloon, Hong Kong, China. Wiesław Ostachowicz, Institute of Fluid-Flow Machinery, Polish Academy of Sciences, 14 Fiszera Street, Gdańsk 80-231, Poland

Besides the existing NDT techniques, approaches relying on vibrations have been rapidly developed in the past decade for the detection of damage in cylinders [7-10]. Damage can cause changes in structural dynamic characteristics; conversely, damage can be identified by such changes [11]. Amongst structural dynamic characteristics, mode shapes can be utilized to graphically characterize the locations and sizes of damage because mode shapes contain the spatial information of damage. With the aid of non-contact vibration measurement via laser scanning, mode shape components (MSCs) acquired from inspection regions of plane structures can be densely measured with high spatial resolutions [12,13].

Structural damage can cause discontinuities in the derivatives of laser-measured MSCs with respect to spatial coordinates, whereby the occurrence, location, and size of the damage can be graphically characterized. Superior to other approaches of damage detection relying on the derivatives of MSCs, the pseudo-force approach has an explicit physical sense and wide applicability to the detection of damage in bars, beams, and plates [14-28]. By rearranging the equation of motion of a structural element, damage-induced perturbation to dynamic equilibrium can be equivalently regarded as a pseudo-force applied to the intact structure. Thereby, the detection of damage can be achieved by identifying the pseudo-force. Starting from the axial dynamic equilibrium, Xu et al. formulated the concept of axial pseudo-force (APF) for the identification of damage in bars [14]. APFs appear in damage regions, whereas they rapidly attenuate and almost vanish at intact locations. Such that damage in bars can be detected and located. By canvassing the damage-induced perturbation to the transverse dynamic equilibrium of a beam element, Xu et al. developed an inverse approach relying on transverse pseudo-force (TPF) to detect a through-width notch in an aluminum beam [15]. By extending dynamic equilibrium from 1D to 2D elements, the 2D TPF was formulated for the detection of damage in plates made of isotropic metals or orthotropic composites [16-21]. Furthermore, to deal with noise interference caused by noise components in measured mode shapes, low-pass wavenumber filtering, multiscale analysis, and "weak" formulation were proposed for denoising [14,16,22,23,24,25,26]. To characterize the full details of multiple damage, integration schemes were developed by fusing pseudo-force-based damage indices (DIs) [19,22,17]. To enable the pseudo-force approach independent of structural and material parameters, the optimization strategy and statistical manner were adopted to establish the baseline-free pseudo-force approach [24,28,19,20].

Although the pseudo-force approach has been widely developed for the identification of damage in plates, there is a noticeable barrier to extending the pseudo-force approach to a cylinder structure such as a wind turbine tower because its radial, longitudinal, and circumferential motions are coupled. To overcome this barrier, this study formulates a new concept of radial pseudo-force (RPF) for the detection of damage in a cylinder structure.

APPROACH OF DAMAGE DETECTION IN CYLINDERS

Consider a cylinder whose vibration is dominated by the radial displacement w. By vanishing the longitudinal displacement u and circumferential displacement v of the cylinder, its equation of radial motion can be approximately written as

$$D\nabla^4 w(x,y,t)+\frac{Eh}{R^2(1-\nu^2)}w(x,y,t)+\rho h\frac{\partial^2 w(x,y,t)}{\partial t^2}=0, \quad (1)$$

where $D=\frac{Eh^3}{12(1-\nu^2)}$ is termed flexural rigidity. By taking account of damping, Equation (1) can be written as

$$D\nabla^4 w(x,y,t)+\frac{Eh}{R^2(1-\nu^2)}w(x,y,t)+\rho h\frac{\partial^2 w(x,y,t)}{\partial t^2}+c\frac{\partial w(x,y,t)}{\partial t}=0. \quad (2)$$

Note that Equation (2) is the same as the equation of out-of-plane motion of a plate when R vanishes.

Considering a cylinder with local damage in a region denoted as Ω, the Young's modulus, thickness, and flexural rigidity of the cylinder can be represented as

$$E(x,y)=\begin{cases}E^I & x,y\notin\Omega\\ E^D & x,y\in\Omega\end{cases},\ h(x,y)=\begin{cases}h^I & x,y\notin\Omega\\ h^D & x,y\in\Omega\end{cases},\ D(x,y)=\begin{cases}D^I & x,y\notin\Omega\\ D^D & x,y\in\Omega\end{cases}, \quad (3)$$

where superscripts I and D indicate the intact and damaged statuses, respectively. By substituting Equation (3) into Equation (2) and rearranging Equation (2), one obtains

$$D^I\nabla^4 w(x,y,t)+\frac{E^I h^I}{R^2(1-\nu^2)}w(x,y,t)+\rho^I h^I\frac{\partial^2 w(x,y,t)}{\partial t^2}+c\frac{\partial w(x,y,t)}{\partial t}=f_{RPF}(x,y), \quad (4)$$

where $f_{RPF}(x,y)$ is the RPF induced by the damage. Theoretically, the RPF exists in the damage region only and vanishes at intact locations:

$$f_{RPF}(x,y)=\begin{cases}0 & x,y\notin\Omega\\ \Delta D\nabla^4 w(x,y,t)+\frac{\Delta E\Delta h}{R^2(1-\nu^2)}w(x,y,t)+\Delta\rho\Delta h\frac{\partial^2 w(x,y,t)}{\partial t^2} & x,y\in\Omega\end{cases}, \quad (5)$$

in which $\Delta E=E^I-E^D$, $\Delta h=h^I-h^D$, $\Delta D=D^I-D^D$, and $\Delta\rho=\rho^I-\rho^D$. For a lightly-damped cylinder with $c\approx 0$, its radial displacement $w(x,y,t)$ is assumed to be the product of the radial mode shape $W(x,y)$ and time response $e^{-\mathrm{i}\omega t}$ with i being the imaginary unit and ω being the natural frequency:

$$w(x,y,t)=W(x,y)e^{-\mathrm{i}\omega t}. \quad (6)$$

By substituting Equation (6) into Equation (4), one obtains

$$D^I\nabla^4 W(x,y)+\left(\frac{E^I h^I}{R^2(1-\nu^2)}-\omega^2\rho^I h^I-\mathrm{i}\omega c\right)W(x,y)=F_{RPF}(x,y), \quad (7)$$

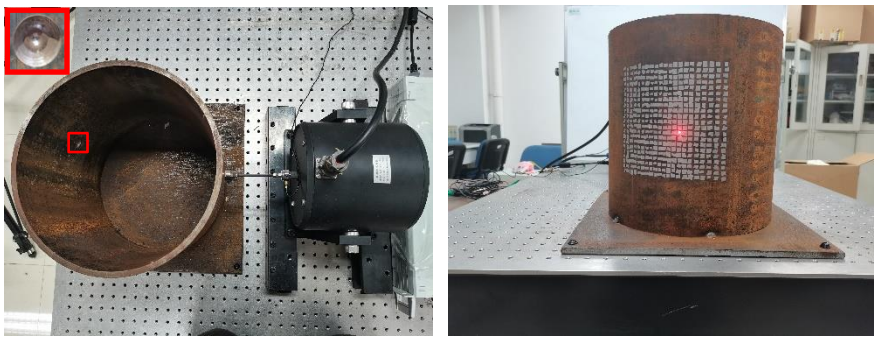

(a) (b)

Figure 1. (a) Electromagnetic shaker attached to the cylinder and (b) laser reflection patches in the inspection region.

in which $F_{RPF}(x,y)$ denotes the amplitude of $f_{RPF}(x,y)$:

$$F_{RPF}(x,y)=\begin{cases}0 & x,y\notin\Omega\\ \Delta D\nabla^4 W(x,y)+(\dfrac{\Delta E\Delta h}{R^2(1-\nu^2)}-\omega^2\Delta\rho\Delta h)W(x,y) & x,y\in\Omega\end{cases}. \tag{8}$$

Note that when the lightly-damped cylinder undergoes steady-state vibration subject to a harmonic excitation at a natural frequency, its operating deflection shape (ODS) of the inspection region approximates the corresponding MSC [29].

Equation (8) indicates that the RPF theoretically appears in the damage region only and almost vanishes in intact locations. Therefore, the RPF is an ideal indicator for the detection of damage in a cylinder. A DI is established in this study using the amplitude of the RPF:

$$DI[x,y]=F_{RPF}[x,y]=\nabla^4 W[x,y]-\lambda^4 W[x,y], \tag{9}$$

where $W[x,y]$ is the discretized $W(x,y)$ and $\lambda^4=\dfrac{1}{D^I}(\omega^2\rho^I h^I+\mathrm{i}\,\omega c-\dfrac{E^I h^I}{R^2(1-\nu^2)})$.

EXPERIMENTAL VALIDATION

A steel cylinder is taken as an experimental specimen of a wind turbine tower model, as shown in Figure 1(a). Considering environmental effects on structural surfaces after long-term service, the surfaces of the specimen have rusted before the experiment. The elastic module and density of the cylinder are 206 GPa and 7850 Kgm^{-3}, respectively. The height and external diameter of the cylinder are both 300 mm. The thickness of the cylinder is 8 mm. The cylinder is welded on a rectangular steel foundation of 10 mm in thickness, which is bolted at four corners on the vibration isolation platform. The internal damage was manufactured by drilling a conical pit on the internal surface of the

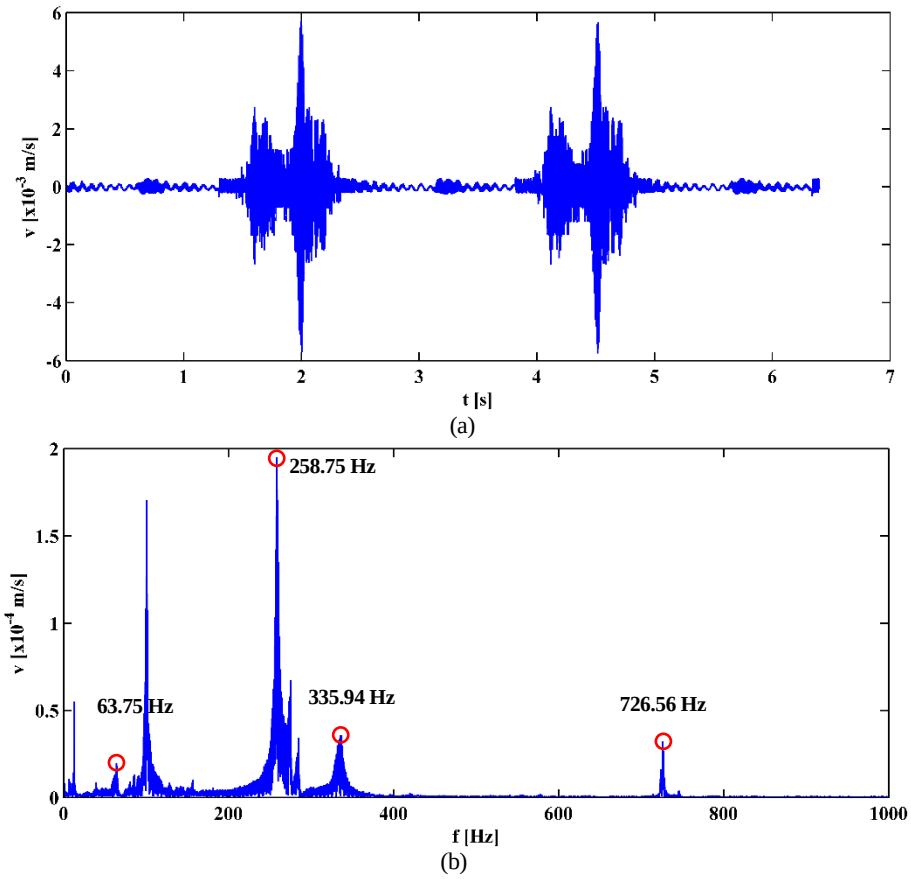

Figure 2. (a) Time history of the velocity response and (b) its frequency spectrum.

cylinder, the center of which is 158 mm from the bottom of the cylinder. The diameter and depth of the conical pit are 20 mm and 4 mm, respectively. As shown in Figure 1(a), the damage is marked in a red box and shown in a zoomed-in view.

An electromagnetic shaker is attached to the external surface of the cylinder to excite it in the radial direction, as shown in Figure 1(a). Simultaneously, the SLV scans over the inspection region to measure the velocities of 21 × 21 measurement points. The size of the inspection region of the cylinder is 160 mm × 160 mm, which spans 70 to 230 mm from the bottom of the cylinder. In dimensionless coordinates of the inspection region, the damage is centered at $\zeta = 0.45$ and $\eta = 0.55$, spanning from 0.3875 to 0.5125 in ζ and from 0.4875 to 0.6125 in η. 21 × 21 reflection patches are pasted on the cylinder to enhance the reflected laser beams, as shown in Figure 1(b).

The modal analysis has been first implemented to acquire the first several natural frequencies of the cylinder. The harmonic excitation periodically sweeps from 0 to 1000 Hz with a period of 2.5 s. Simultaneously, the velocity response of the cylinder is measured from the upper right corner of the inspection region. The time history of the velocity response in two sweeping periods is shown in Figure 2(a), and its frequency spectrum is obtained by the fast Fourier transform (FFT) and shown in Figure 2(b).

The cylinder is excited at its resonances to obtain large magnitudes for high signal-to-noise ratios. From the frequency spectrum in Figure 2(b), the natural frequencies of the cylinder at 63.75, 258.75, 335.94, and 726.56 Hz are selected as the excitation frequencies. In comparison with numerical simulation results, vibrations of the cylinder

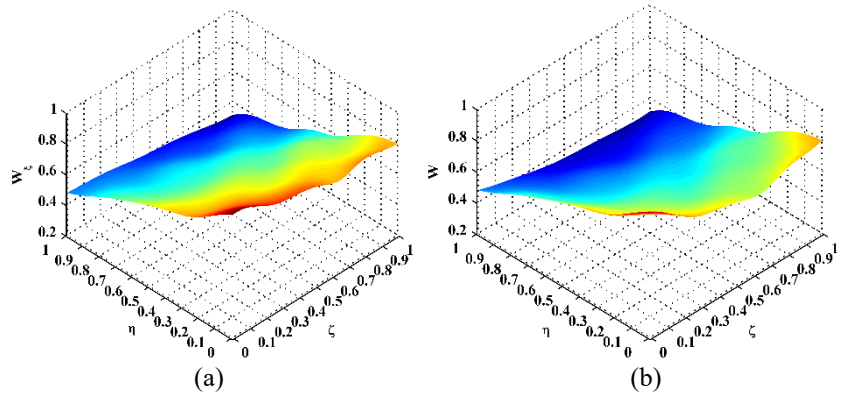

Figure 3. (a) Measured and (b) radial ODSs associated with the natural frequency of 63.75 Hz.

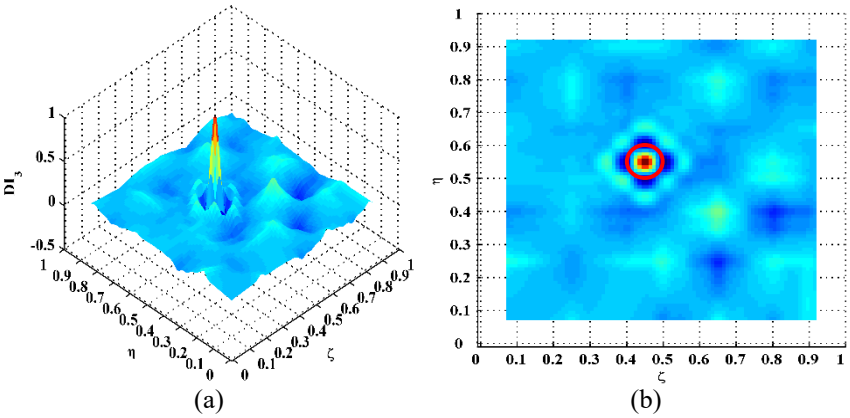

Figure 4. (a) DI and (b) its planform (the outline of the actual damage region is marked in a red circle).

that correspond to those natural frequencies are dominated by the radial components. When the cylinder undergoes harmonic vibrations subject to the harmonic excitations, the SLV pointwisely scans the entire inspection region to measure the velocities. Taking the scenario of 63.75 Hz for illustration purposes, the measured ODS (Figure 3(a)) is corrected to radial ODS (Figure 3(b)) by the geometric relationship. Note that the measured ODS needs to be denoised by the wavelet transform [30]. To increase the spatial resolution, the radial ODS is extended from 21 × 21 to 101 × 101 by cubic interpolation. As the cylinder is lightly damped, the ODS can be regarded as the corresponding MSC. By Equation (9), the DI is obtained and shown in Figure 4. The DI rapidly attenuates and almost vanishes at intact locations; meanwhile, the occurrence of the damage can be evidently manifested by a sharply rising peak in the damage region. In its planform, the peak concentrated in the damage region graphically characterizes the damage: the identified damage is centered at $\zeta = 0.45$ and $\eta = 0.55$, spanning from about 0.4 to 0.5 in ζ and from about 0.5 to 0.6 in η, respectively. The result of damage identification corresponds to the actual damage region, whose outline is marked in a red circle.

CONCLUSIONS

Addressing the barrier to extending the pseudo-force approach to a cylinder, a new concept of RPF is formulated for the detection of damage in cylinder structures such as wind turbine towers. The RPF-based approach is experimentally validated on an experimental specimen of a wind turbine tower model. The experimental results reveal that the approach is capable of graphically characterizing the occurrence, location, and size of damage in a cylinder structure.

ACKNOWLEDGMENTS

This work is supported by the Fundamental Research Funds for the Central Universities through Grant Nos. B210201034 and B220204002.

REFERENCES

1. Leissa, A. W. and Qatu, M. S. 2011. Vibration of Continuous Systems. McGraw Hill, New York.
2. Wen, J., Xia, Z., and Choy, F. 2011. "Damage detection of carbon fiber reinforced polymer composites via electrical resistance measurement," *Composites: Part B*, 42: 77-86.
3. Zalamedaa, J. N., Winfreea, W. P., Seebob, J. P., and Johnston, P. H. 2011. "Thermography inspection for detection and tracking of composite cylinder damage during load testing," *AIP Conference Proceedings*, 1335(1): 450-457.
4. Na, S. and Lee, H. K. 2012. "Resonant frequency range utilized electro-mechanical impedance method for damage detection performance enhancement on composite structures," *Composite Structures*, 94(8): 2383-2389.
5. Ji, M., He, J., Lai, Y., and Xiao, R. 2015. "Application of laser ultrasonic visualization inspection in the detection of cylinder sleeve," in International Conference on Mechatronics, Electronic, Industrial and Control Engineering, Shenyang, China.
6. Mercuri, A., Fanelli, P., Ubertini, S., Falcucci, G., and Biscarini, C. 2021. "Effect of strain measurement layout on damage detection and localization in a free falling compliant cylinder impacting a water surface," *Fluids*, 6(2): 58.
7. Rucka, M. and Wilde, K. 2010. "Neuro-wavelet damage detection technique in beam, plate and shell structures with experimental validation," *Journal of Theoretical and Applied Mechanics*, 48(3): 579-604.
8. Hu, H., Wu, C., and Lu, W. J. 2011. "Damage detection of circular hollow cylinder using modal strain energy and scanning damage index methods," *Computers and Structures*, 89(1-2): 149-160.
9. Taajobian, M., Mohammadzaheri, M., Doustmohammadi, M., Amouzadeh, A., and Emadi, M. 2018. "Fault diagnosis of an automobile cylinder head using low frequency vibrational data," *Journal of Mechanical Science and Technology*, 32(7): 3037-3045.
10. Miller, B. and Ziemianski, L. 2021. "Detection of material degradation of a composite cylinder using mode shapes and convolutional neural networks," *Materials*, 14(21): 6686.
11. Fan, W. and Qiao, P. 2011. "Vibration-based damage identification methods A review and comparative study," *Structural Health Monitoring-An International Journal*, 10(1): 83-111.
12. Chen, D. M., Xu, Y. F., and Zhu, W. D. 2018. "Non-model-based multiple damage identification of beams by a continuously scanning laser Doppler vibrometer system," *Measurement*, 115: 185-196.
13. Cao, S., Lu, Z., Wang, D., and Xu, C. 2021. "Robust multi-damage localization in plate-type structures via adaptive denoising and data fusion based on full-field vibration measurements," *Measurement*, 178: 109393.
14. Xu, W., Zhu, W., Su, Z., Cao, M., and Xu, H. 2021. "A novel structural damage identification approach using damage-induced perturbation in longitudinal vibration," *Journal of Sound and Vibration*, 496(1-2): 115932.
15. Xu, H., Cheng, L., Su, Z., and Guyader, J-L. 2011. "Identification of structural damage based on

locally perturbed dynamic equilibrium with an application to beam component," *Journal of Sound and Vibration*, 330(24): 5963-5981.
16. Xu, H., Cheng, L., Su, Z., and Guyader, J-L. 2013. "Damage visualization based on local dynamic perturbation: Theory and application to characterization of multi-damage in a plane structure," *Journal of Sound and Vibration*, 332(14): 3438-3462.
17. Xu, H., Cheng, L., and Su, Z. 2013. "Suppressing influence of measurement noise on vibration-based damage detection involving higher-order derivatives," *Advances in Structural Engineering*, 16(1): 233-244.
18. Xu, H., Zhou, Q., Cao, M., Su, Z., and Wu, Z. 2018. "A dynamic equilibrium-based damage identification method free of structural baseline parameters experimental validation in a two-dimensional plane structure," *Journal of Aerospace Engineering*, 31(6): 04018081.
19. Cao, S., Ouyang, H., and Chen, L. 2019. "Adaptive damage localization based on locally perturbed dynamic equilibrium and hierarchical clustering," *Smart Materials and Structures*, 28(7): 075003.
20. Cao, M. S., Su, Z., Xu, H., Radzieński, M., Xu, W., and Ostachowicz, W. 2020. "A novel damage characterization approach for laminated composites in the absence of material and structural information," *Mechanical Systems and Signal Processing*, 143(3-4):106831.
21. Li, T., Cao, M., Li, J., Yang, L., Xu, H., and Wu, Z. 2021. "Structural Damage Identification Based on Integrated Utilization of Inverse Finite Element Method and Pseudo-Excitation Approach," *Sensors*, 21(2): 606.
22. Xu, H., Su, Z., Cheng, L., Guyader, J-L., and Hamelin, P. 2013. "Reconstructing interfacial force distribution for identification of multi-debonding in steel-reinforced concrete structures using noncontact laser vibrometry," *Structural Health Monitoring-An International Journal*, 12(5-6): 507-521.
23. Cao, M., Cheng, L., Su, Z., and Xu, H. 2012. "A multi-scale pseudo-force model in wavelet domain for identification of damage in structural components," *Mechanical Systems and Signal Processing*, 28:638–659.
24. Cao, M., Su, Z., Cheng, L., and Xu, H. 2013. "A multi-scale pseudo-force model for characterization of damage in beam components with unknown material and structural parameters," *Journal of Sound and Vibration*, 332(21): 5566-5583.
25. Xu, H., Su, Z., Cheng, L., and Guyader, J-L. 2015. "A "Pseudo-excitation" approach for structural damage identification: From "Strong" to "Weak" modality," *Journal of Sound and Vibration*, 337: 181-198.
26. Zhang, C., Ji, H., Qiu, J., Cheng, L., Yao, W., and Wu, Y. 2020. "A local specific stiffness identification method based on a multi-scale "weak" formulation," *Mechanical Systems and Signal Processing*, 140: 106650.
27. Deng, A., Cao, M., Lu, Q., and Xu, W. 2021. "Identification of multiple cracks in composite laminated beams using perturbation to dynamic equilibrium," *Sensors*, 21(18): 6171.
28. Xu, H., Zhou, Q., Cao, M., Su, Z., and Wu, Z. 2018. "A dynamic equilibrium-based damage identification method free of structural baseline parameters experimental validation in a two-dimensional plane structure," *Journal of Aerospace Engineering*, 31(6): 04018081.
29. Schwarz, B. J. and Richardson, M. H. 1999. "Introduction to operating deflection shapes," *CSI Reliability Week*, 10: 121-126.
30. Mallat, S. 2008. A Wavelet Tour of Signal Processing. Academic Press, San Diego.